The Journal of Thoracic and Cardiovascular Surgery
2024 掲載予定

主論文
（著者投稿最終版）

Therapeutic potential of human iPS cell-derived cardiac tissue in an ischemic model with unloaded condition mimicking left ventricular assist device

Daisuke Heima[a,b,e], MD; Masafumi Takeda[b,f], MD, PhD; Yasuhiko Tabata[d], PhD, D.Med.Sci, D.Pharm; Kenji Minatoya[a], MD, PhD; Jun K. Yamashita[b,g,*], MD, PhD; Hidetoshi Masumoto[a,c,*], MD, PhD

[a] Department of Cardiovascular Surgery, Graduate School of Medicine, Kyoto University, Kyoto, Japan

[b] Department of Cell Growth and Differentiation, Center for iPS Cell Research and Application, Kyoto University, Kyoto, Japan

[c] Clinical Translational Research Program, RIKEN Center for Biosystems Dynamics Research, Kobe, Japan

[d] Department of Biomaterials, Institute for Frontier Life and Medical Sciences, Kyoto University, Kyoto, Japan

[e] Present affiliation: Department of Cardiovascular Surgery, Kansai Medical University, Hirakata, Japan

17 [f] Present affiliation: Department of Cardiology, Saiseikai Hyogoken Hospital, Kobe,

18 Japan

19 [g] Present affiliation: Department of Cellular and Tissue Communications, Graduate

20 School of Medicine, The University of Tokyo. Tokyo, Japan

21

22 **Conflict of Interest Statement**

23 J.K.Y. is a founder, equity holder, and scientific adviser of iHeart Japan Corporation. J.

24 K.Y. and H.M. are co-inventors on multiple pluripotent stem cell-related patents.

25

26 **Funding**

27 This work was supported by grants from Japan Agency for Medical Research and

28 Development (AMED) under Grant Number JP18he0702246 (to H.M., Y.T., J.K.Y. and

29 K.M.).

30

31 **Animal experiments**

32 All experimental procedures were carried out in accordance with the animal care
33 guidelines established by Kyoto University and the "*Guide for the Care and Use of*
34 *Laboratory Animals*" published by the National Institutes of Health. All animal
35 experimental protocols were approved by the Animal Experimentation Committee of
36 Kyoto University (#Med Kyo 15261).

37

38 ***Corresponding authors:**
39 Hidetoshi Masumoto, MD, PhD
40 Department of Cardiovascular Surgery, Graduate school of Medicine, Kyoto University
41 54 Kawahara-cho, Shougoin, Sakyo-ku, Kyoto 606-8507, Japan
42 Phone: +81-75-751-3784
43 E-mail: masumoto@kuhp.kyoto-u.ac.jp

44

45 Jun K. Yamashita, MD, PhD
46 Department of Cellular and Tissue Communications, Graduate School of Medicine, The
47 University of Tokyo
48 7-3-1, Hongo, Bunkyo-ku, Tokyo 113-0033, Japan
49 Phone: +81-3-5800-9430
50 E-mail: juny@m.u-tokyo.ac.jp

51

52 **Word Count:** 4434 words

53

54 **Glossary of Abbreviations:**

55 CTSs = cardiac tissue sheets

56 hiPSC = Human induced pluripotent stem cell

57 HiCT = hiPSC-derived cardiac tissue

58 HTx = heterotopic heart transplantation

59 ICM = ischemic cardiomyopathy

60 LVAD = left ventricular assist device

61 MI = myocardial infarction

62 MuRF-1 = muscle-specific RING finger 1

63 PCM1 = pericentriolar material 1

64 SERCA2a = sarcoplasmic/endoplasmic reticulum Ca^{2+}-ATPase 2a

65 VAD = ventricular assist device

66

67 **Central picture legend:**

68 HiCT transplant on unloaded heart reduces infarct remodeling and promotes graft
69 survival.
70
71 **Central message:**
72 HiCTs transplantation to ischemic hearts under unloading condition promotes graft
73 survival, attenuates infarct remodeling, promotes neovascularization and prevents
74 atrophy of cardiomyocytes.
75
76 **Perspective Statement:**
77 HiCT treatment holds potential as an effective treatment for ischemic hearts supported by
78 ventricular assist devices (VADs). It can promote graft survival, reduce infarct
79 remodeling, stimulate neovascularization, and attenuate cardiomyocyte atrophy. These
80 findings suggest that HiCT treatment could serve as a "bridge to recovery" strategy for
81 VAD patients.
82

ABSTRACT

Objective: This study aimed to explore the therapeutic potential of hiPSC-derived cardiac tissues (HiCTs) in the emerging approach of "Bridge to recovery (BTR)" for severe heart failure with ventricular assist devices (VADs). We utilized a rat model of heterotopic heart transplantation (HTx) to mimic VAD support and heart unloading.

Methods: HiCTs were created by inserting gelatin hydrogel microspheres between cell sheets made from hiPSC-derived cardiovascular cells. Male athymic nude rats underwent myocardial infarction (MI) and were divided into the following groups: MI (loaded, untreated control), MI+HTx (unloaded, untreated control), MI+HTx+HiCT (unloaded, treated), and MI+HiCT (loaded, treated). HiCTs were placed on the epicardium of the heart in treated groups. We evaluated HiCT engraftment, fibrosis, neovascularization using histological analysis.

Results: After four weeks, HiCTs successfully engrafted in five out of six rats in the MI+HTx+HiCT group (83.3%). The engrafted HiCT area was greater under unloaded conditions (MI+HTx+HiCT) than loaded conditions (MI+HiCT) ($P<0.05$).

MI+HTx+HiCT had a significantly smaller infarct area compared to MI and MI+HTx. The MI+HTx+MiCT group exhibited higher vascular density in the border zone than MI and MI+HTx. HiCT treatment suppressed cardiomyocyte atrophy due to LV unloading (P=0.001). The protein level of MuRF1, an atrophy-related ubiquitin ligase, was lower in the MI+HTx+HiCT group than MI+HTx (P=0.036). However, HiCT treatment did not significantly improve LV systolic function in unloaded hearts.

Conclusions: Transplanting HiCTs into ischemic hearts under unloaded conditions promoted engraftment, neovascularization, attenuated infarct remodeling, and suppressed myocyte atrophy. These results suggest that HiCT treatment could contribute to future advancements in BTR. (250 words)

Key words:

Ventricular assist device; stem cell; bridge to recovery.

114 **INTRODUCTION**

115

116 Cardiovascular disease continues to be the primary cause of death globally[1]. Within this
117 category, ischemic heart disease (IHD) is responsible for most common cases of heart
118 failure with reduced ejection fraction[2, 3]. While heart transplantation is an effective
119 treatment for patients with end-stage heart failure who are unresponsive to other therapies,
120 the scarcity of heart donors limits the widespread application of this therapeutic option
121 for the majority of individuals suffering from severe heart failure.

122 One of the palliative therapies for end-stage heart failure is the use of a
123 ventricular assist device (VAD)[4] . The implantation of a VAD allows heart failure patients
124 to survive by maintaining systemic circulation. Clinically, VADs have been employed as
125 a bridging measure for heart transplantation while patients wait for a suitable donor
126 (bridge to transplantation), as well as a lifelong circulatory support (destination therapy)[5,
127 6]. Additionally, recent investigations have focused on "bridge to recovery (BTR)", which
128 is another option for utilizing VADs. BTR involves a multidisciplinary approach aimed
129 at anticipating functional recovery of the failing heart by combining VAD support.

130 Studies in animal models[7, 8] and clinical settings[9] have reported that left ventricular (LV)
131 unloading through VADs can restore cardiac gene expression and reduce LV dilatation,
132 along with other biomedical interventions.

133 In research aimed at achieving BTR, attempts have been made with gene
134 therapy or stem cell transplantation[10, 11]. It is assumed that the combination therapy of
135 VAD therapy and cell transplantation not only provides an additive effect through LV
136 unloading with the VAD therapy and the paracrine effect of cell therapy but also offers a
137 synergistic effect where mechanical unloading creates a favorable condition for cell
138 transplantation. It has been reported that the unloading condition improved the
139 engraftment efficiency of cardiac stem cells in an infarcted heart during mouse
140 heterotopic heart transplantation (HTx) model[12]. However, the reported clinical trials of
141 BTR utilizing stem cell transplantation have so far fallen short of expectations in terms
142 of the success rate of the strategy, including functional recovery and weaning from VAD
143 support[6, 13, 14].

144 In our previous studies, we reported that transplanting human induced
145 pluripotent stem cell (hiPSC)-derived cardiac tissue sheets (CTSs) containing

146 cardiomyocytes, vascular endothelial cells, and vascular mural cells into rat and pig
147 subacute myocardial infarction (MI) models resulted in improved cardiac function by
148 attenuating infarct remodeling and promoting angiogenesis[15, 16]. Additionally, we
149 observed a higher therapeutic and myocardial regenerative effect in epicardial
150 transplantation of human iPS cell-derived cardiac tissue (HiCT) onto a rat MI model[17],
151 which involved layering CTSs using gelatin hydrogel microspheres (the gelatin hydrogel
152 microsphere layer and the cell layer exist adjacent to each other rather than being mixed)
153 to enhance oxygen and nutrient supply within the thick tissue[18, 19]. Transplanting HiCT
154 onto patients undergoing VAD therapy may hold promise as a new strategy for bridge to
155 recovery (BTR).

156 In this study, we examined the impact of transplanting HiCT onto an unloaded
157 rat heart, mimicking VAD support, and evaluated the potential for bridge to recovery
158 (BTR) in the experimental model. Additionally, we assessed the biological effects of
159 HiCT treatment on the unloaded heart, including graft survival and infarct remodeling.

160

161 **MATERIAL AND METHODS**

162

163 Detailed methods are provided as Supporting Information online.

164

165 **Experimental protocol**

166 All experimental procedures were carried out in accordance with the animal care

167 guidelines established by Kyoto University and the "*Guide for the Care and Use of*

168 *Laboratory Animals*" published by the National Institutes of Health. All animal

169 experimental protocols were approved by the Animal Experimentation Committee of

170 Kyoto University (#Med Kyo 15261).

171 The time course of the experiment is illustrated in Figure 1A. The rats that

172 successfully developed myocardial infarction (MI), characterized by fractional shortening

173 less than 40%, were divided into the following groups: (1) MI group (n=6) (loaded,

174 untreated control) underwent no HTx. A laparotomy was performed, and the abdominal

175 aorta was exposed as a sham operation for HTx. (2) MI+HTx group (n=31) (unloaded,

176 untreated control) underwent HTx. Sixteen rats survived after HTx. (3) MI+HTx+HiCT

177 group (n=28) (unloaded, treated) underwent HTx followed by HiCT treatment. Seventeen

178 rats survived after HTx. For the comparison of engraftment of HiCT with or without

179 unloading, we added a group as follows: (4) MI+HiCT group (n=5) (loaded, treated).

180 They did not undergo HTx but received HiCT treatment. The comparisons are explained

181 in Figure 1B and Figure 5A. The experimental group is presented in Supplemental Figure

182 1.

183

184 **Human iPSC-derived cardiac tissue (HiCT) formation**

185 The cardiovascular cells differentiated from hiPSC line (201B6) were dissociated and

186 then plated onto a 10% fetal bovine serum (FBS)-coated 12-multiwell UpCell (CellSeed,

187 Tokyo, Japan) at a density of 10-12 × 10^5 cells per well. After 4 days in culture, the cells

188 were transferred to room temperature to allow for the detachment of monolayer cell sheets.

189 The size of the collected cell sheets was almost identical in every experimental repeats.

190 It was then plated onto a Matrigel-coated 6-cm dish, and 0.5 mg of gelatin hydrogel

191 microspheres[17, 18] dissolved in phosphate-buffered saline (PBS) was placed on the surface

192 of the cell sheet. After 45 minutes, another monolayer cell sheet was stacked on top of

193 the previous one. This stacking process was repeated 4 times, resulting in a five-layered

194 cell sheet known as human iPSC-derived cardiac tissue (HiCT) (Figure 1C).

195

196 **Flow cytometry**

197 The monolayer cell sheet was dissociated and then stained with surface markers specific

198 for each cell lineage. The cellular components of monolayer cell sheets before preparation

199 of the HiCTs included 52.0±4.9 % of cardiac isoform of troponin-T (cTnT)-positive

200 cardiomyocytes, 6.5±2.2 % of vascular endothelial (VE)-cadherin-positive vascular

201 endothelial cells, 8.8±4.9 % of platelet-derived growth factor receptor beta (PDGFRβ)-

202 positive vascular mural cells and 0.3±0.1 % of TRA-1-60-positive undifferentiated cells,

203 respectively (Figure 1D).

204

205 **Subacute MI rat model**

206 Male athymic nude rats (F344/N Jcl-rnu/rnu, CLEA Japan, Inc., Tokyo, Japan) aged 12-

207 17 weeks were utilized as donors and recipients for transplantation, respectively. The MI

208 model rats were generated following previously described methods[15].

209

210 **Heterotopic heart transplantation and HiCT treatment**

211 Heterotopic heart transplantation was performed following previously established
212 methods[20]. Briefly, one week after creating the MI, the donor rat was anesthetized, the
213 right and left superior vena cava and IVC were ligated, and 5 mL of cold cardioplegia
214 solution (Miotector; Mochida, Tokyo, Japan) were injected from the ascending aorta for
215 cardioprotection. Once cardiac arrest was achieved, the infarcted heart and lung were
216 harvested and preserved in cold cardioplegia solution. Next, the recipient rat was
217 anesthetized and underwent laparotomy. The ascending aorta of the donor heart was
218 anastomosed end-to-side to the recipient rat abdominal aorta. After reperfusion, the
219 transplanted heart spontaneously resumed beating immediately. In the MI+HTx+HiCT
220 group, the HiCT was placed on the epicardium of the MI region and manually spread to
221 cover the entire area of the infarction (Figure 1E).

222

223 **Histological analysis**

224 Hearts were harvested 4 weeks after HTx (5 weeks after MI induction). The animals were
225 anesthetized with 1% isoflurane while placed on a volume cycled ventilator for small
226 animals. After opening the chest and abdomen, 100 ml of heparinized cold saline (500
227 IU) followed by 50 mL of 4% paraformaldehyde (PFA) were infused through the apex of
228 the recipient's heart. The heterotopically transplanted heart in the abdomen was rapidly
229 excised and placed in 4% PFA overnight. Afterward, it was embedded in OCT compound
230 (Sakura Finetek Japan, Tokyo, Japan) and frozen. The tissue was transversely sliced into
231 7 μm sections just below the ligation point and subjected to Hematoxylin-Eosin and
232 Masson trichrome staining, as well as immunofluorescence staining. For
233 immunofluorescence staining, the sections were treated with Protein Block Serum Free
234 (DAKO, Glostrup, Danish) and incubated overnight with primary antibodies at 4°C. Anti-
235 mouse Alexa 546 (1:500) and anti-rabbit Alexa 488 (Invitrogen, Eugene, OR, USA)
236 (1:400) were used as secondary antibodies. The area of engrafted human cells was
237 manually traced as positive cell clusters, identified by staining with anti-cTnT antibody
238 (rabbit polyclonal; Abcam, Cambridge, UK; 1:500) and human nuclear antibody (HNA)
239 (mouse monoclonal, clone 235-1; Millipore, Billerica, MA, USA; 1:200). To evaluate the

240 proliferation of transplanted cardiomyocytes, double-positive cells stained with anti-Ki67
241 antibody (rabbit monoclonal, clone D3B5; Cell Signaling Technology, Danvers, MA,
242 USA) and anti-cTnT antibody (rabbit polyclonal antibody; Thermo Fisher Scientific,
243 Waltham, MA, USA; 1:500) were visualized. The length of fibrotic lesions at the
244 endocardium level and the total length of the endocardium were manually traced and
245 measured using Masson's trichrome-stained sections, and the ratio of the MI length to the
246 total length was calculated for each section. The MI area was measured as the ratio of the
247 area of fibrotic lesions to left ventricular myocardium. The area of fibrotic lesion and left
248 ventricular myocardium were manually traced and measured using Masson's trichrome-
249 stained sections. We established a standardized criterion by preparing one section at the
250 same location for each rat, specifically just below the permanent ligation thread of the
251 coronary artery introduced during MI induction. Wall thickness was calculated as the
252 average of five randomly selected vertical distances of the wall (including both ends) in
253 the MI area. For vascular density (number of vessels/mm^2), four views of the border zone
254 (two views on each side) were selected from vWF-stained sections, and the number of
255 vessels was manually counted in each view. A rabbit polyclonal vWF antibody (DAKO;

256 1:1000) was used as the primary antibody for vWF staining. A mouse monoclonal cTnT
257 antibody (clone 13211, Thermo Fisher Scientific; 1:500) was used for double staining
258 with cTnT and vWF. To measure the size of cardiomyocytes, five views of the non-
259 infarcted area in the left ventricle were selected from Pericentriolar Material 1 (PCMI)
260 and eosin-stained sections. The size of cardiomyocytes was calculated from randomly
261 selected 50 cardiomyocytes (10 cardiomyocytes in each view) whose nuclei were stained
262 with anti-PCMI antibody (a cardiomyocyte nuclear marker[21]) and whose cytoplasmic
263 membrane appeared intact and had a round shape. For PCMI staining, a rabbit polyclonal
264 antibody (Thermo Fisher Scientific; 1:400) was used as the primary antibody. Images
265 were captured using an all-in-one digital microscope (BIOREVO BZ-9000; Keyence,
266 Osaka, Japan) and analyzed using the BZ-X Analyzer (Keyence) software and ImageJ[22]
267 (U.S. National Institutes of Health, Bethesda, MD, USA).
268

269 **Statistical analysis**

270 The data were analyzed using GraphPad Prism software for Mac (version 7.0, San Diego,
271 California, USA). The results are presented as mean ± standard deviation. Comparisons

272 between two groups were performed using the unpaired t-test or Mann-Whitney test.
273 Comparisons among three groups were carried out using one-way analysis of variance
274 (ANOVA) followed by Tukey's test as a post hoc analysis. The correlation was assessed
275 using Pearson's correlation coefficient. A p-value of less than 0.05 was considered
276 statistically significant.
277
278 **RESULTS**
279
280 **Baseline surgical data**
281 The baseline echocardiogram data prior to MI induction are presented in Supplemental
282 Table 1. The survival rate following MI induction and subsequent heterotopic
283 transplantation is illustrated in Supplemental Figure 1. As demonstrated in Supplemental
284 Table 2, there were no significant differences in cardiac function among the three groups
285 of rats enrolled in the study, as confirmed by echocardiography one week after MI.
286 Additionally, there were no significant differences in the total operation time of whole
287 host and recipient surgeries, operation time for recipient rats (transplantation time), and

288 the time from donor heart resection to reperfusion of the transplanted heart (ischemic
289 time) (Figure 1F).
290
291 **Engraftment after HiCT transplantation onto a rat MI model**
292 Immunofluorescent staining revealed successful engraftment of transplanted HiCTs,
293 covering the infarcted region in 5 out of 6 rats in the MI+HTx+HiCT group, four weeks
294 after transplantation (Figure 2A,B). Almost all engrafted HiCTs consisted of HNA-
295 positive human cells, with the majority being cardiac troponin-T (cTnT)-positive
296 cardiomyocytes. Additionally, we observed a higher content of Ki67-positive
297 cardiomyocyte nuclei in the engrafted HiCTs compared to the native myocardium of rats,
298 even at 4 weeks after HiCT treatment (Figure 2C). We confirmed that proliferating cells
299 remained on the epicardium and did not penetrate into the myocardium. These findings
300 suggest that HiCTs are successfully engrafted after transplanted into unloaded hearts, and
301 the engrafted cardiomyocytes retain their ability to proliferate in the absence of
302 mechanical loading.
303

304 **HiCT transplantation for unloaded heart attenuated infarct remodeling after MI**

305 Subsequently, we assessed the extent of infarct remodeling following MI under each
306 condition. The hearts in the MI group exhibited fibrosis extension and thinning of the
307 infarcted wall five weeks after MI, indicating the progression of infarct remodeling
308 (Figure 3A). However, the ratio of MI length to total LV length was significantly reduced
309 in the MI+HTx+HiCT group compared to the other two groups [MI vs. MI+HTx vs
310 MI+HTx+HiCT: 33.69±6.26 vs. 34.56±8.49 vs. 22.43±5.51%; P=0.032 (MI vs
311 MI+HTx+HiCT), 0.021 (MI+HTx vs MI+HTx+HiCT)] (Figure 3B). The percentage of
312 MI area in whole LV area was significantly reduced in MI+HTx+HiCT group compared
313 to that in MI+HTx group [MI vs MI+HTx vs MI+HTx+HiCT: 21.99±4.63 vs 28.08±7.10
314 vs 19.05±4.05%; P=0.028 (MI+HTx vs MI;HTx+HiCT)] (Figure 3C). On the other hand,
315 the wall thickness of the MI+HTx group tended to be thicker and was significantly thicker
316 in the MI+HTx+HiCT group compared to the MI group [MI vs. HTx vs. MI+HTx+HiCT:
317 0.761±0.129 vs. 1.295±0.294 vs. 1.570±0.562 mm; P=0.063 (MI vs MI+HTx), 0.005 (MI
318 vs MI+HTx+HiCT)] (Figure 3D). These results indicate that heterotopic transplantation

319 tends to preserve LV wall thickness following MI, and HiCT treatment under unloading

320 conditions attenuates infarct remodeling after MI.

321

322 **HiCT treatment under unloaded condition promoted neovascularization in border**

323 **zone of MI**

324 We previously have reported that the limited extent of infarct remodeling observed with

325 HiCT treatment is due to the promotion of neovascularization in the border zone of the

326 MI mediated by the engrafted HiCTs in loaded hearts[17]. Here, we examined the vascular

327 density in the border zone following HiCT treatment. There was no significant difference

328 in vascular density of the border zone between the MI group and the MI+HTx group.

329 However, the MI+HTx+HiCT group exhibited a higher vascular density in the border

330 zone compared to the other two groups [MI vs. MI+HTx vs. MI+HTx+HiCT: 12.8±4.728

331 vs. 16.07±1.684 vs. 70.54±58.35/mm^2; P=0.025 (MI vs MI+HTx+HiCT), 0.035

332 (MI+HTx vs MI+HTx+HiCT)] (Figure 4A, B). Furthermore, there was a correlation

333 between vascular density and the area of engrafted HiCTs in the MI+HTx+HiCT group

334 (R^2=0.756, P=0.0245) (Figure 4C). These results suggest that HiCT treatment under

335 unloaded conditions promotes neovascularization in the border zone, and the extent of
336 neovascularization might be mediated by the engrafted HiCTs. Additionally, we
337 confirmed that neovascularization was also promoted in the adjacent region (Figure 4D)
338 and within the engrafted HiCTs (Figure 4E), supporting the notion that
339 neovascularization aids in the engraftment of HiCTs.
340

341 **Enhancement of the engraftment efficiency of HiCT in the unloaded heart**

342 Next, we examined how the unloaded condition affect the efficiency of the HiCT
343 engraftment. We compared the efficiency of HiCT engraftment between under unloaded
344 condition (MI+HTx+HiCT group) and under loaded condition (MI+HiCT group) (Figure
345 5A). In MI+HiCT group, only 3 out of 5 transplanted HiCT (60%) were engrafted 4 weeks
346 after transplantation, while 5 out of 6 transplanted HiCT (83%) were engrafted in
347 MI+HTx+HiCT group. The engrafted area in MI+HTx+HiCT group was significantly
348 larger than that in MI+HiCT group (MI+HiCT vs MI+HTx+HiCT: 0.216±0.229 vs
349 0.841±0.632mm^2; P=0.0498) (Figure 5B,C). These results indicate that the unloaded
350 condition is more desirable for the engraftment of HiCT than loaded condition. The

351 positive ratio of Ki-67 (Figure 5D) was equivalent with that of engrafted HiCTs in
352 unloaded heart (Figure 2C), indicating that the proliferation of cardiomyocytes is not
353 affected by the loaded condition.
354
355 **HiCT treatment attenuates the atrophy of cardiomyocytes under unloaded**
356 **condition**
357 According to reports, long-term LVAD implantation has been found to cause atrophy of
358 cardiomyocytes[23]. Therefore, we conducted an investigation to examine how HiCT
359 treatment under unloading conditions affects the progression of cardiomyocyte atrophy
360 caused by unloading. As illustrated in Figures 6A and 6B, the cross-sectional area of
361 cardiomyocytes in the non-infarcted area was significantly smaller in the MI+HTx group
362 compared to the MI+HTx+HiCT group (MI+HTx vs MI+HTx+HiCT: 336±72.2 vs
363 622±139 μm^2; P=0.001). Previous studies have reported that atrophy of skeletal muscle
364 and myocardium during unloading is partly attributed to increased degradation of muscle
365 protein triggered by the activation of the ubiquitin-proteasome system during unloading[23,
366 24]. Consequently, we examined the protein expression level of muscle-specific RING

367 finger 1 (MuRF-1), which is one of the ubiquitin ligases associated with muscle atrophy.

368 In the MI+HTx+HiCT group, the protein expression level of MuRF-1 was significantly

369 lower than that in the MI+HTx group (MI+HTx vs MI+HTx+HiCT: 0.953±0.734 vs

370 0.197±0.185; P=0.036) (Figures 6C,D). These findings suggest that HiCT treatment

371 under unloading conditions mitigated cardiomyocyte atrophy by suppressing the

372 activation of MuRF-1 protein expression during unloading.

373

374 **DISCUSSION**

375

376 In this study, we demonstrated the therapeutic potential of HiCT treatment in a rat

377 subacute MI model under unloaded conditions (Figure 7). This was achieved by

378 attenuating infarct remodeling, which we previously reported to be mediated by the

379 promotion of neovascularization under loaded conditions as well[15, 16]. Furthermore, we

380 observed a significantly greater efficiency in the engraftment of HiCTs under unloaded

381 conditions as opposed to loaded conditions, which would further enhance the therapeutic

382 mechanisms. These findings suggest that HiCT treatment may offer a potential solution

383 for BTR, and it could be a viable therapeutic approach to simultaneously perform
384 epicardial transplantation of HiCTs during VAD implantation aiming to BTR. The
385 unloaded hearts showing preserved MI wall thickness (Figures 3A, D) would also provide
386 an advantage for functional recovery through HiCT treatment compared to the loaded
387 condition. It is worth noting that weaning from VAD is rare and mostly observed in
388 younger patients with non-ischemic cardiomyopathy or those with acute conditions like
389 myocarditis, rather than patients with ischemic cardiomyopathy[25-28]. Therefore, HiCT
390 treatment could emerge as a novel approach to enhance BTR for ischemic
391 cardiomyopathy. However, it is important to note that we were unable to observe
392 significant improvement in LV function by the HiCT treatment because it was technically
393 demanding to evaluate cardiac function of the heterotopically implanted hearts located in
394 abdominal region which may hinder the realization of a complete BTR approach based
395 solely on this strategy. Furthermore, in order to translate the treatment approach in this
396 study into practical applications for clinical BTR, it is necessary to go beyond using
397 subacute myocardial infarction models like the one employed in this study. We may need
398 to verify the therapeutic effects by including models of chronic ischemic cardiomyopathy

399 with fully developed scar tissue, and non-ischemic cardiomyopathy. Additionally, a more
400 extended period of observation after treatment would be required to further assess
401 whether HiCT transplantation therapy can indeed contribute to the clinical BTR.

402 Regarding the engraftment efficiency of HiCTs, it was found that the unloaded
403 condition yielded better results compared to the loaded condition. This aligns with a study
404 by Kurazumi et al., who reported an increased efficiency of cell engraftment in a mouse
405 model when cardiac stem cells were intramyocardially injected under unloaded
406 conditions[12]. In our study, we explored tissue sheet transplantation on the surface of the
407 heart and demonstrated that the unloaded condition was favorable even for this method,
408 as it led to improved engraftment of transplanted cells. We assume there are two reasons
409 for this result. First, the transplanted cells may benefit from improved blood supply under
410 unloaded conditions. Watanabe et al. conducted a study using a pig model of ischemic
411 heart failure and reported that the implantation of temporary ventricular support device
412 (IMPELLA®) improved blood flow to the coronary artery[29]. This suggests that the
413 presence of a circulatory support device creates a better host condition for cell
414 transplantation. In chronic heart failure, systemic perfusion decreases due to low cardiac

415 function or underlying ischemic heart diseases affecting coronary arterial perfusion.
416 Therefore, it is assumed that the unloaded condition provides a more favorable
417 environment for the host heart, enhancing the efficiency of transplanted cell engraftment
418 through increased coronary blood flow facilitated by circulatory support. Here, we made
419 an intriguing discovery that neovascularization facilitated by HiCT treatment also
420 supported the engraftment of HiCTs. This was evidenced by the observation that the
421 engrafted area showed a correlation with the density of capillaries in the border zone
422 (Figure 4C). Moreover, we observed enhanced neovascularization in the adjacent region
423 and inside the engrafted HiCTs (Figures 4D,E). It is possible that the improved
424 engraftment of HiCTs not only attenuated infarct remodeling but also sequentially
425 promoted neovascularization, thereby enhancing the host condition for engraftment.
426 Another reason is that the removal of LV distension through unloading might create a
427 more favorable environment for cell transplantation. In a failing heart, the LV experiences
428 excessive pressure and volume, resulting in tension on the LV wall[30] which may hinder
429 the survival of the cells. In a state of cardiac overload, it is suggested that mitochondrial
430 production is promoted, leading to the activation of reactive oxygen species production

431 which may promote cell death[31]. It would be possible that by relieving the pressure and
432 volume overload, the tension on the transplanted HiCT is reduced, leading to an improved
433 engraftment efficiency of HiCT.

434 In our research, we discovered that HiCT treatment effectively reduced the
435 atrophy of cardiomyocytes in the non-infarcted area under unloaded conditions. Some
436 studies have previously reported that the implantation of a VAD in an unloaded condition
437 can morphologically restore hypertrophic cardiomyocytes caused by cellular remodeling
438 after myocardial infarction[32, 33]. However, other reports have suggested that this change
439 leads to the atrophy of cardiomyocytes under unloaded conditions[23]. This notion is further
440 supported by research showing the atrophy of cardiomyocytes in a normal goat heart after
441 VAD transplantation[34]. Additionally, another study found that the ventricular volume of
442 a rat normal heart decreased by 60% one month after heterotopic heart transplantation[35].
443 The underlying mechanism behind this atrophy is believed to be the activation of atrophy-
444 related ubiquitin ligases, which are specific to skeletal and cardiac muscles. These ligases
445 promote the degradation of cardiac proteins under unloaded conditions[23]. In fact, studies
446 have shown an increase in atrophy-related ubiquitin ligase expression in heterotopically

447 transplanted mouse hearts and human hearts equipped with LVADs after unloading[36]. In
448 our study, we found that the HiCT treatment onto unloaded hearts exhibited lower
449 expression of MuRF-1, one of the atrophy-related ubiquitin ligases, compared to the
450 hearts without HiCT treatment. These results indicate that HiCT treatment under
451 unloaded conditions suppresses the atrophy of cardiomyocytes in the non-infarcted area
452 by attenuating the protein expression of MuRF-1. This suppression of atrophy, a major
453 drawback of long-term LVAD support, may increase the likelihood of successful BTR.

454 There are several limitations in the present study. First, in our current research,
455 we attempted to replicate the physiological state of an unloaded heart supported by LVAD
456 using a rat heterotopic transplantation model. However, this model does not fully replicate
457 the cardiac physiology of the hearts supported by LVAD in a clinical context. To address
458 this challenge, as the next step in our study, we believe it is necessary to assess the effects
459 of HiCT transplantation in a setting more closely resembling the clinical use of LVAD,
460 possibly by utilizing a LVAD implantation model in large animals. Second, due to
461 technical complexities, we were unable to assess the function of the transplanted heart in
462 this study. To explore the potential for BTR through HiCT transplantation, it would be

463 desirable to demonstrate an improvement in cardiac function with an unloaded heart
464 mediated by HiCT transplantation, which can be considered a limitation in this study. In
465 future experiments using large animals and LVAD implantation, rather than heterotopic
466 transplantation, we plan to accurately evaluate how HiCT transplantation has affected
467 cardiac function.
468
469 **CONCLUSIONS**
470
471 Transplanting HiCTs into ischemic hearts while in an unloaded condition has been shown
472 to enhance neovascularization, reduce infarct remodeling, and prevent cardiomyocyte
473 atrophy caused by unloading, a disadvantage associated with long-term LVAD
474 implantation. Additionally, the engraftment efficiency of HiCTs was found to be higher
475 under unloaded conditions compared to loaded conditions. These findings suggest that
476 HiCT treatment has the potential to effectively treat ischemic hearts supported by LVAD
477 and may serve as a strategy for achieving a BTR for VAD in the future.
478

ACKNOWLEDGMENTS

The authors thank Mr. Shuichi Miyake (Kyoto University) for providing expert technical assistance. The authors thank Dr. Hemant Poudyal (Kyoto University) for valuable advises for the functional evaluations.

Declaration of generative AI and AI-assisted technologies in the writing process

During the preparation of this work the authors used ChatGPT in order to improve language and readability, with caution. After using this tool/service, the authors reviewed and edited the content as needed and take full responsibility for the content of the publication.

492 **REFERENCES**

493

494 1. World Health Organization (WHO) Global Health Estimates: Life expectancy and

495 leading causes of death and disability.

496 https://www.who.int/data/gho/data/themes/mortality-and-global-health-estimates.

497 2. Tsao CW, Aday AW, Almarzooq ZI, et al. Heart Disease and Stroke Statistics-

498 2023 Update: A Report From the American Heart Association. *Circulation.*

499 2023;147:e93-e621.

500 3. Glynn P, Lloyd-Jones DM, Feinstein MJ, Carnethon M, Khan SS. Disparities in

501 Cardiovascular Mortality Related to Heart Failure in the United States. *J. Am. Coll.*

502 *Cardiol.* 2019;73:2354-2355.

503 4. Miller RJH, Teuteberg JJ, Hunt SA. Innovations in Ventricular Assist Devices for

504 End-Stage Heart Failure. *Annu. Rev. Med.* 2019;70:33-44.

505 5. Yuzefpolskaya M, Schroeder SE, Houston BA, et al. The Society of Thoracic

506 Surgeons Intermacs 2022 Annual Report: Focus on the 2018 Heart Transplant

507 Allocation System. *Ann. Thorac. Surg.* 2023;115:311-327.

508 6. Kirklin JK, Naftel DC, Pagani FD, et al. Seventh INTERMACS annual report:
509 15,000 patients and counting. *J. Heart Lung Transplant.* 2015;34:1495-1504.
510 7. Tsuneyoshi H, Oriyanhan W, Kanemitsu H, et al. Heterotopic transplantation of
511 the failing rat heart as a model of left ventricular mechanical unloading toward
512 recovery. *ASAIO J.* 2005;51:116-120.
513 8. Muranaka H, Marui A, Tsukashita M, et al. Prolonged mechanical unloading
514 preserves myocardial contractility but impairs relaxation in rat heart of dilated
515 cardiomyopathy accompanied by myocardial stiffness and apoptosis. *J. Thorac.*
516 *Cardiovasc. Surg.* 2010;140:916-922.
517 9. Hall JL, Birks EJ, Grindle S, et al. Molecular signature of recovery following
518 combination left ventricular assist device (LVAD) support and pharmacologic
519 therapy. *Eur. Heart J.* 2007;28:613-627.
520 10. Tseng CC, Ramjankhan FZ, de Jonge N, Chamuleau SA. Advanced Strategies for
521 End-Stage Heart Failure: Combining Regenerative Approaches with LVAD, a
522 New Horizon? *Front Surg.* 2015;2:10.

523 11. Ibrahim M, Rao C, Athanasiou T, Yacoub MH, Terracciano CM. Mechanical
524 unloading and cell therapy have a synergistic role in the recovery and regeneration
525 of the failing heart. *Eur. J. Cardiothorac. Surg.* 2012;42:312-318.
526 12. Kurazumi H, Li TS, Takemoto Y, et al. Haemodynamic unloading increases the
527 survival and affects the differentiation of cardiac stem cells after implantation into
528 an infarcted heart. *Eur. J. Cardiothorac. Surg.* 2014;45:976-982.
529 13. Ascheim DD, Gelijns AC, Goldstein D, et al. Mesenchymal precursor cells as
530 adjunctive therapy in recipients of contemporary left ventricular assist devices.
531 *Circulation.* 2014;129:2287-2296.
532 14. Stempien-Otero A, Helterline D, Plummer T, et al. Mechanisms of bone marrow-
533 derived cell therapy in ischemic cardiomyopathy with left ventricular assist device
534 bridge to transplant. *J. Am. Coll. Cardiol.* 2015;65:1424-1434.
535 15. Masumoto H, Ikuno T, Takeda M, et al. Human iPS cell-engineered cardiac tissue
536 sheets with cardiomyocytes and vascular cells for cardiac regeneration. *Sci. Rep.*
537 2014;4:6716.

538 16. Ishigami M, Masumoto H, Ikuno T, et al. Human iPS cell-derived cardiac tissue
539 sheets for functional restoration of infarcted porcine hearts. *PLoS One.*
540 2018;13:e0201650.
541 17. Osada H, Kawatou M, Fujita D, et al. Therapeutic potential of clinical-grade
542 human induced pluripotent stem cell-derived cardiac tissues. *JTCVS Open.*
543 2021;8:359-374.
544 18. Tabata Y, Nagano A, Muniruzzaman M, Ikada Y. In vitro sorption and desorption
545 of basic fibroblast growth factor from biodegradable hydrogels. *Biomaterials.*
546 1998;19:1781-1789.
547 19. Matsuo T, Masumoto H, Tajima S, et al. Efficient long-term survival of cell grafts
548 after myocardial infarction with thick viable cardiac tissue entirely from
549 pluripotent stem cells. *Sci. Rep.* 2015;5:16842.
550 20. Wang J, Tsukashita M, Nishina T, et al. Chronic partial unloading restores beta-
551 adrenergic responsiveness and reverses receptor downregulation in failing rat
552 hearts. *J. Thorac. Cardiovasc. Surg.* 2009;137:465-470.

553 **21.** Bergmann O, Zdunek S, Alkass K, Druid H, Bernard S, Frisen J. Identification of
554 cardiomyocyte nuclei and assessment of ploidy for the analysis of cell turnover.
555 *Exp. Cell Res.* 2011;317:188-194.
556 **22.** Schneider CA, Rasband WS, Eliceiri KW. NIH Image to ImageJ: 25 years of
557 image analysis. *Nat Methods.* 2012;9:671-675.
558 **23.** Hill JA, Olson EN. Cardiac plasticity. *N. Engl. J. Med.* 2008;358:1370-1380.
559 **24.** Rudrappa SS, Wilkinson DJ, Greenhaff PL, Smith K, Idris I, Atherton PJ. Human
560 Skeletal Muscle Disuse Atrophy: Effects on Muscle Protein Synthesis,
561 Breakdown, and Insulin Resistance-A Qualitative Review. *Front. Physiol.*
562 2016;7:361.
563 **25.** Birks EJ, Tansley PD, Hardy J, et al. Left ventricular assist device and drug
564 therapy for the reversal of heart failure. *N. Engl. J. Med.* 2006;355:1873-1884.
565 **26.** Goldstein DJ, Maybaum S, MacGillivray TE, et al. Young patients with
566 nonischemic cardiomyopathy have higher likelihood of left ventricular recovery
567 during left ventricular assist device support. *J. Card. Fail.* 2012;18:392-395.

568 **27.** Simon MA, Kormos RL, Murali S, et al. Myocardial recovery using ventricular
569 assist devices: prevalence, clinical characteristics, and outcomes. *Circulation.*
570 2005;112:I32-36.
571 **28.** Mano A, Nakatani T, Oda N, et al. Which factors predict the recovery of natural
572 heart function after insertion of a left ventricular assist system? *J. Heart Lung*
573 *Transplant.* 2008;27:869-874.
574 **29.** Watanabe S, Fish K, Kovacic JC, et al. Left Ventricular Unloading Using an
575 Impella CP Improves Coronary Flow and Infarct Zone Perfusion in Ischemic
576 Heart Failure. *J Am Heart Assoc.* 2018;7.
577 **30.** Tonnessen T, Knudsen CW. Surgical left ventricular remodeling in heart failure.
578 *Eur. J. Heart Fail.* 2005;7:704-709.
579 **31.** Canseco DC, Kimura W, Garg S, et al. Human ventricular unloading induces
580 cardiomyocyte proliferation. *J. Am. Coll. Cardiol.* 2015;65:892-900.
581 **32.** Diakos NA, Selzman CH, Sachse FB, et al. Myocardial atrophy and chronic
582 mechanical unloading of the failing human heart: implications for cardiac assist
583 device-induced myocardial recovery. *J. Am. Coll. Cardiol.* 2014;64:1602-1612.

584 **33.** Zafeiridis A, Jeevanandam V, Houser SR, Margulies KB. Regression of cellular
585 hypertrophy after left ventricular assist device support. *Circulation.* 1998;98:656-
586 662.
587 **34.** Kinoshita M, Takano H, Takaichi S, Taenaka Y, Nakatani T. Influence of
588 prolonged ventricular assistance on myocardial histopathology in intact heart. *Ann.*
589 *Thorac. Surg.* 1996;61:640-645.
590 **35.** Brinks H, Tevaearai H, Muhlfeld C, et al. Contractile function is preserved in
591 unloaded hearts despite atrophic remodeling. *J. Thorac. Cardiovasc. Surg.*
592 2009;137:742-746.
593 **36.** Baskin KK, Rodriguez MR, Kansara S, et al. MAFbx/Atrogin-1 is required for
594 atrophic remodeling of the unloaded heart. *J. Mol. Cell. Cardiol.* 2014;72:168-
595 176.
596
597 **FIGURE LEGENDS**
598
599 **FIGURE 1: Heterotopic heart transplantation and HiCT transplantation.**

600 **(A)** The time course of the experiments. **(B)** Schema of surgical groups. **(C)**
601 Represenrarive Macroscopic appearance of HiCT. Scale bar: 1 cm. **(D)** Cellular
602 components of monolayer cell sheets before preparation of HiCTs (n=8). **(E)**
603 Representative surgical appearance of HTx and HiCT transplantation. **(F)** Duration of
604 surgeries. WB, Western blotting; MI, myocardial infarction; HTx, heterotopic heart
605 transplantation; HiCT, human iPS-derived cardiac tissue sheets; CM, cardiomyocyte; EC,
606 vascular endothelial cell: MC, vascular mural cell; cTnT, cardiac isoform of troponin-T;
607 VE-cad, vascular-endothelial cadherin; PDGFRb, platelet-derived growth factor receptor
608 beta.
609
610 **FIGURE 2: Myocardial regeneration after HiCT transplantation onto unloaded**
611 **hearts.**
612 **(A-C)**, Immunohistochemical analysis for engrafted HiCTs. **(A)** Representative
613 immunostaining for HiCT on the surface of transplanted heart. HNA (red), cTnT (green)
614 and DAPI (blue). Scale bars: 1 mm. **(B)** Higher magnification [dashed square in **(A)**].
615 Scale bars: 50 μm. **(C)** Representative immunostaining for Ki67 (green), cTnT (red), and

616 DAPI (blue) for engrafted HiCT and native rat myocardium. White dotted lines indicate

617 the margin of engrafted HiCT which was confirmed by consecutive sections stained with

618 HNA and cTnT. Yellow arrows indicate Ki67 and cTnT double-positive cells. Scale bar:

619 100 μm. HNA, human nucleic antigen; DAPI, 4',6-diamidino-2-phenylindole.

620

621 **FIGURE 3: HiCT transplantation attenuates left ventricular remodeling after MI**

622 **in unloaded hearts.**

623 **(A)** Representative Masson's Trichrome staining of rat hearts 4weeks after HTx. Scale

624 bars: 1 mm **(B)** The ratio of MI length of Total length. **(C)** The ratio of MI area to the

625 total area of left ventricle**. (D)** Wall thickness.

626

627 **FIGURE 4: Neovascularization after HiCT transplantation onto unloaded MI**

628 **hearts.**

629 **(A)** Representative immunostaining at 4 weeks after transplantation at border zone. vWF

630 (green), cTnT (red), and DAPI (blue). Engrafted region of HiCT is not shown. Scale bars:

631 100 μm. **(B)** Vascular number (diameter <100 μm) per 1mm^2. **(C)** Correlation between

632 engrafted area and vascular density. **(D,E)** Representative immunostaining for

633 neovascularization at adjacent region of HiCT **(D)** and inside of HiCT **(E**; White arrow).

634 White dotted line indicates the border of the engrafted region. Scale bars: 100 μm.

635

636 **FIGURE 5: Comparison of engrafted area of HiCT between loaded and unloaded**

637 **MI hearts.**

638 **(A)** Schema of surgical groups. **(B)** Representative immunostaining for HiCTs. HNA

639 (red), cTnT (green) and DAPI (blue). Scale bars: 1 mm. **(C)** Quantitation of engrafted

640 area. **(D)** Representative immunostaining for Ki67 (green), cTnT (red), and DAPI (blue)

641 for engrafted HiCT and native rat myocardium. Yellow arrows indicate Ki67 and cTnT

642 double-positive cells. Scale bars: 100 μm.

643

644 **FIGURE 6: Attenuation of cardiomyocyte atrophy after HiCT transplantation onto**

645 **unloaded MI hearts.**

646 **(A)** Representative histological staining of cardiomyocytes for PCM1 immunostaining

647 and eosin. Black enclosed lines indicate single cardiomyocyte. Scale bars: 100 μm. **(B)**

648 Cross section area of cardiomyocytes (n=50 each). **(C)** Representative Western blotting

649 for MuRF-1. **(D)** MuRF-1/ß-actin protein level. PCM1, Pericentriolar material 1; MuRF-

650 1, muscle-specific RING finger 1.

651

652 **FIGURE 7: Schema of the research.**

653 We utilized a rat model of heterotopic heart transplantation (HTx) to mimic VAD support

654 and heart unloading, investigating the therapeutic potential of hiPSC-derived cardiac

655 tissues (HiCTs) for severe heart failure with left ventricular assist devices (LVADs).

656

657 **VIDEO LEGEND**

658

659 **VIDEO 1: Surgical procedure of the rat heterotopic heart transplantation model.**

660

661

662

663

664 **Graphical abstract**

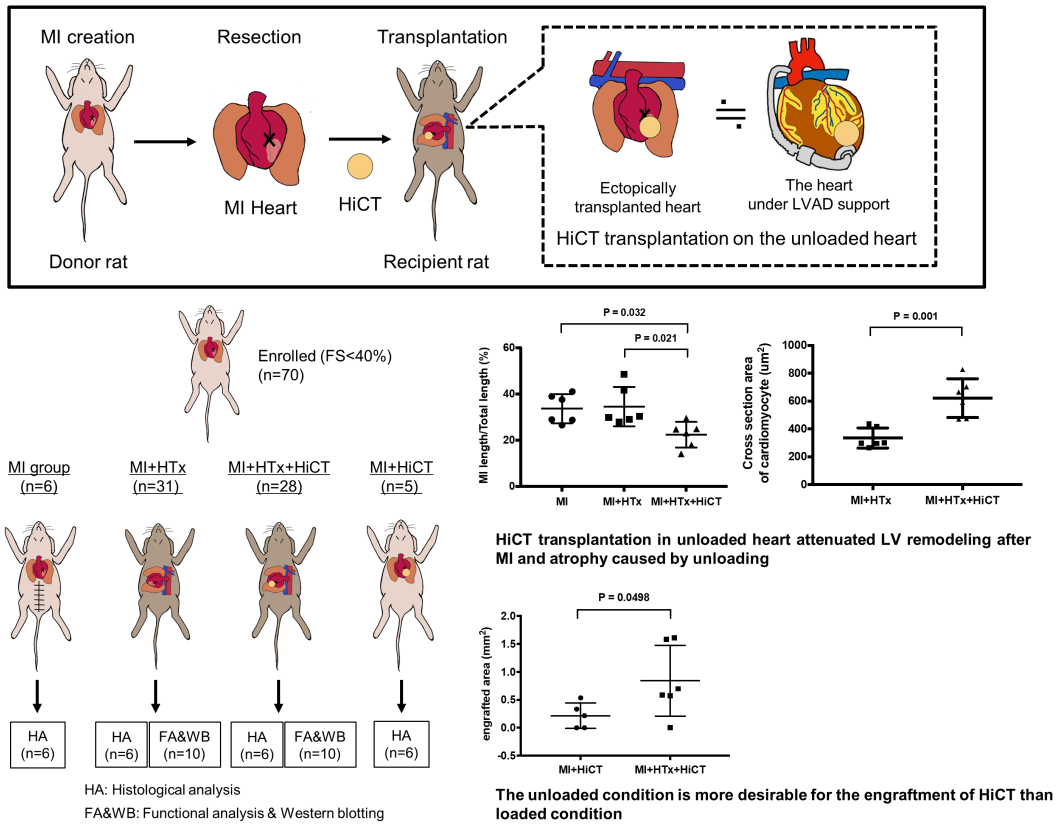

665

666

667

668

669

670

671

672

673 **Central picture**

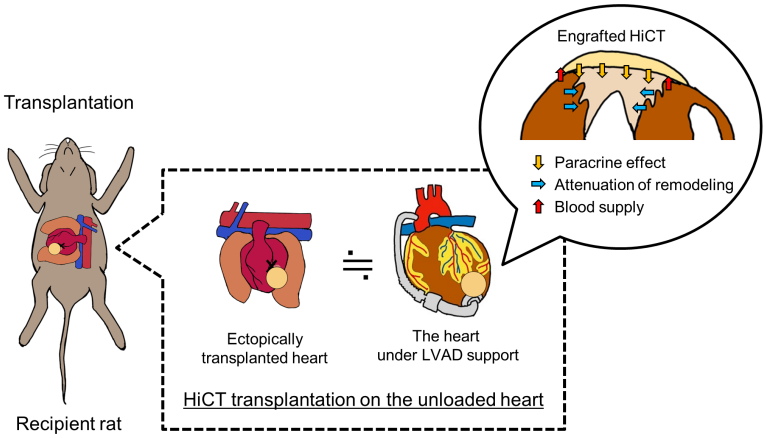

674

675

676

677

678

679

680

681

682 **Figure1**

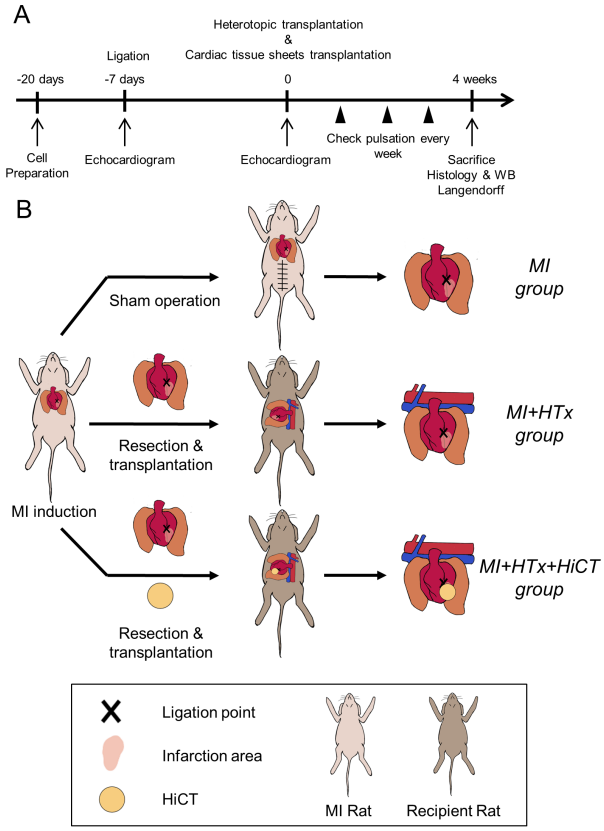

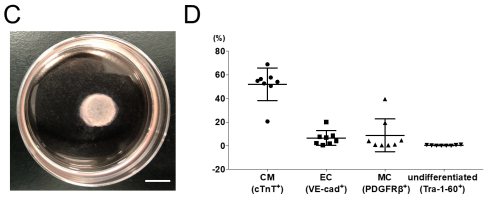

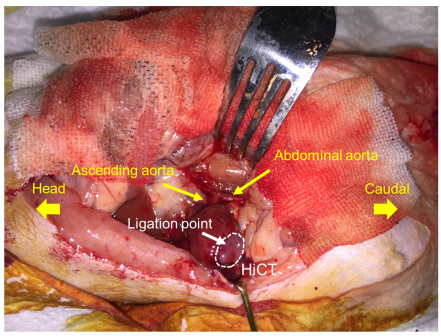

F

Operation data

	Total operation Time (min)	Transplantation Time (min)	Ischemic time (min)
MI+HTx group (n=16)	57.6±7.7	39.7±6.2	28.7±3.1
MI+HTx+HiCT group (n=17)	59.2±5.5	42.5±3.9	27.9±4.5
P value	0.49	0.12	0.58

683

684

685

686

687

688

689

690

691 **Figure2**

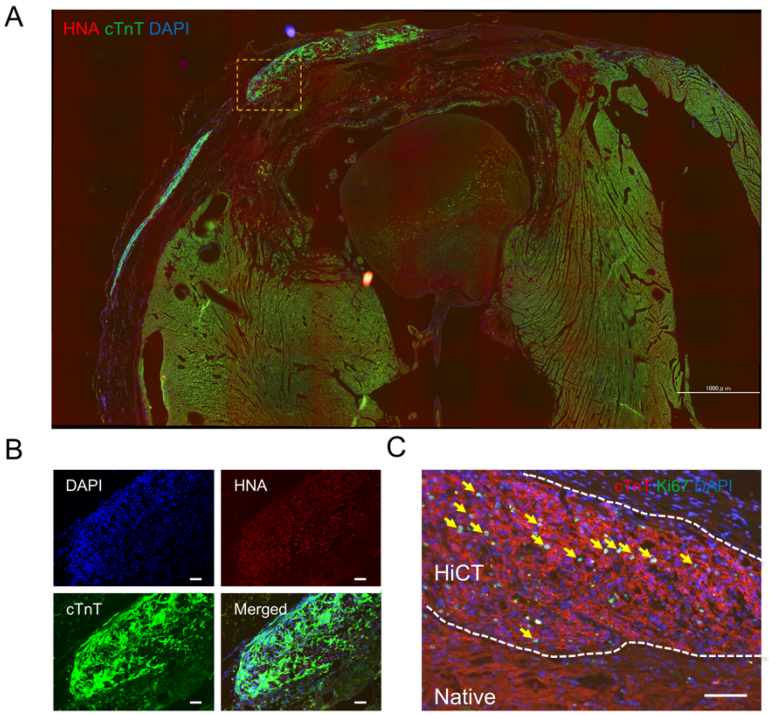

692

693

694

695

696

697

698

699

700 **Figure3**

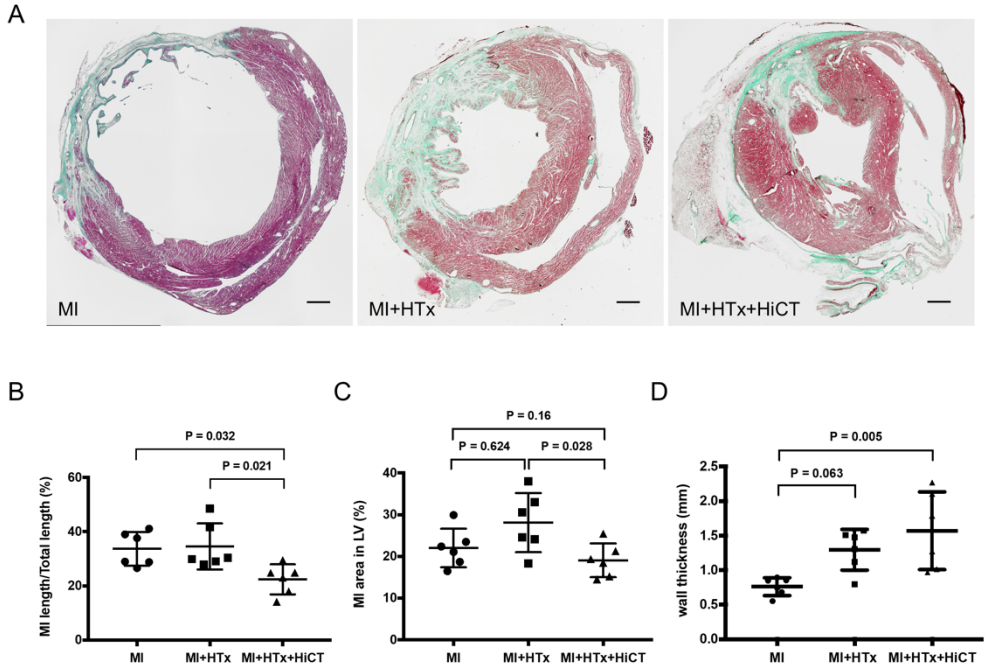

701

702

703

704

705

706

707

708

709 **Figure4**

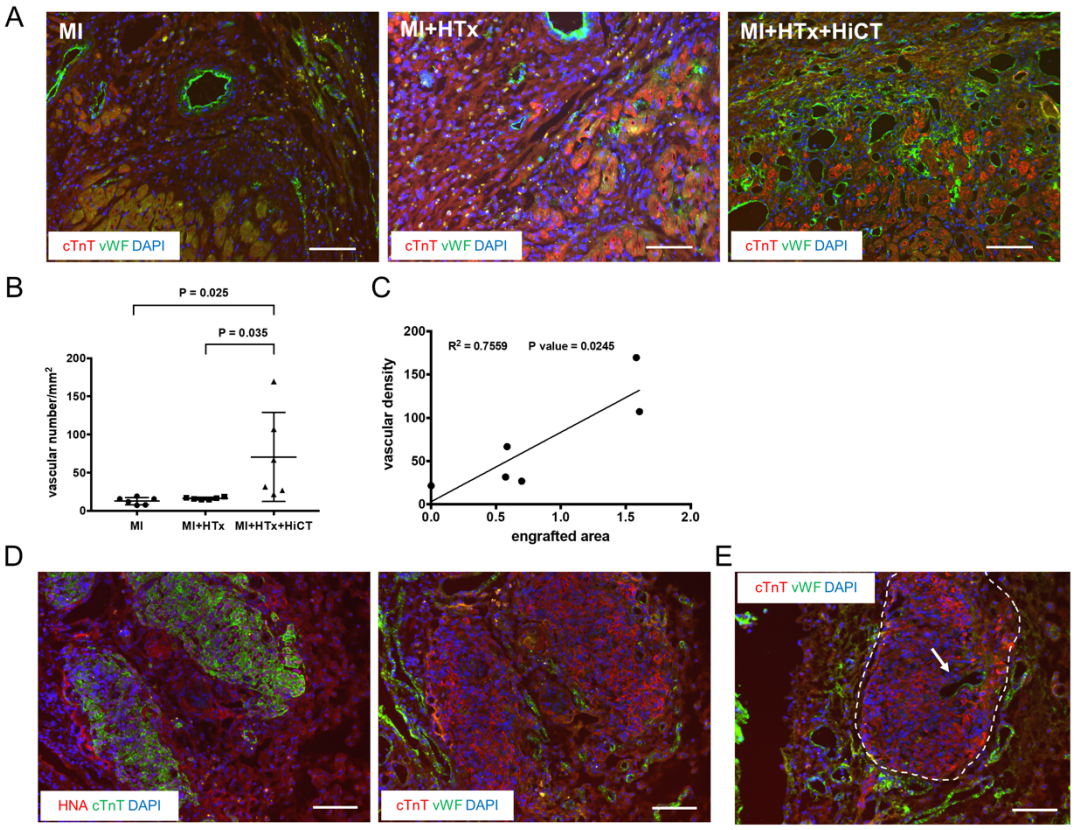

710

711

712

713

714

715

716

717

718 **Figure5**

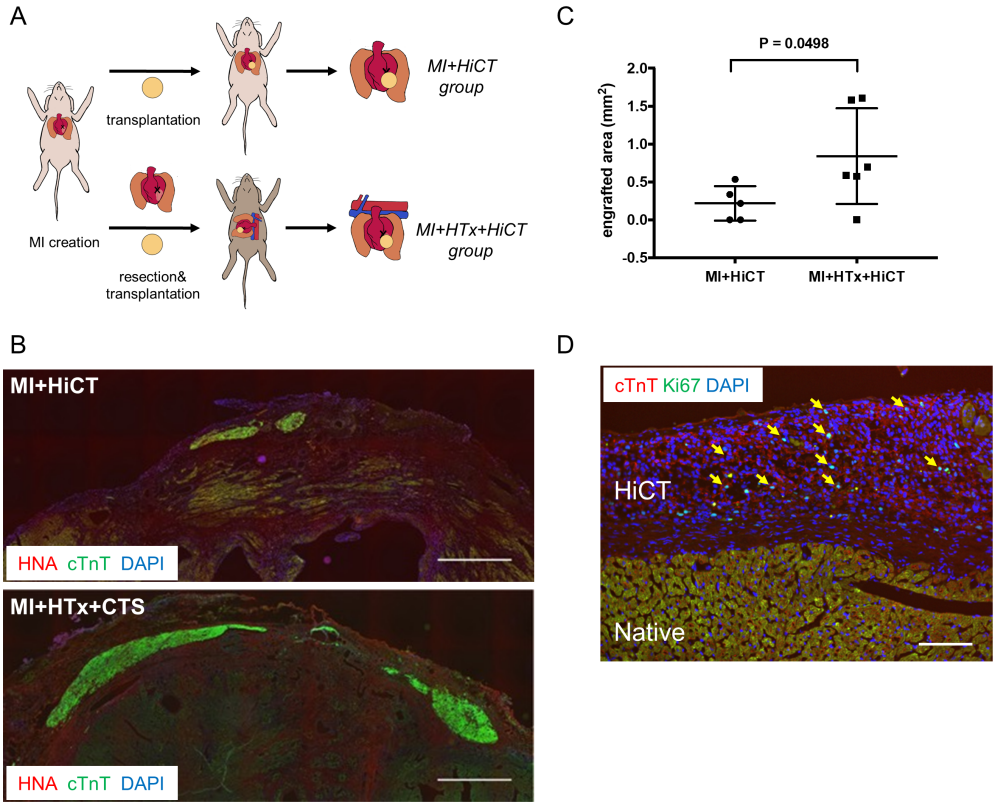

719

720

721

722

723

724

725

726

727 **Figure6**

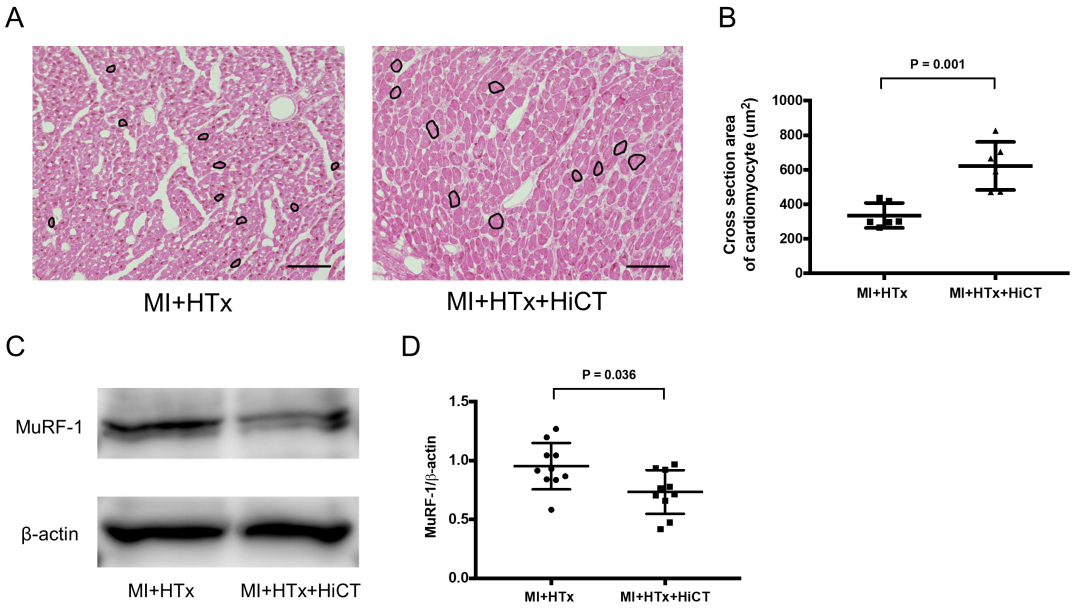

728

729

730

731

732

733

734

735

736 **Figure7**

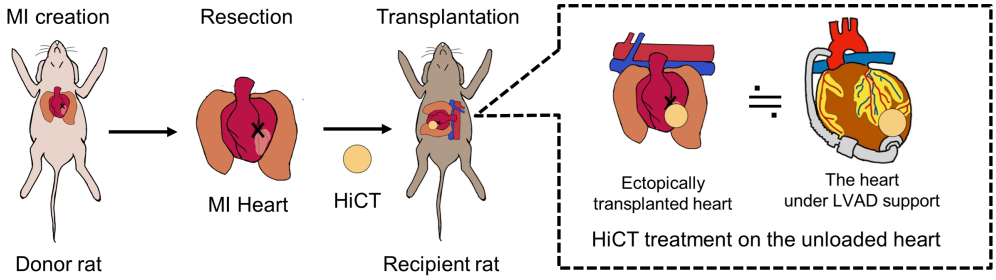

737

738